

# Simultaneous separation of simulated radionuclides strontium and neodymium using in situ hydrotalcite synthesis

Shaoming Yu · Caicun Zha · Feifei Lu ·  
Xiaodong Wei · Kanglin Wang

Received: 15 January 2013 / Published online: 9 April 2013  
© Akadémiai Kiadó, Budapest, Hungary 2013

**Abstract** The simulated radionuclides Sr and Nd were simultaneously separated from high level liquid waste (HLLW) using in situ hydrotalcite synthesis. The optimum conditions of removal of Sr and Nd determined by acid–base titration, single factor test and X-ray powder diffraction (XRD) are that the initial  $C_{Nd(III)}$ , initial  $C_{Sr(II)}$ , pH range and (Sr + Mg)/(Nd + Al) molar ratio are 70, 90 mg L<sup>-1</sup>, 10–11 and around 3, respectively. Both the removal rates of Sr and Nd could reach more than 99 % under these conditions. The synthetic samples were characterized by XRD, Fourier transform infrared spectroscopy, scanning electron microscope. The results indicate that as-synthesized samples possess single hydrotalcite phase, which confirms that Sr and Nd separated from HLLW are all embedded into the crystal lattice of Sr–Nd-HTlc. In addition, the morphology of Sr–Nd-HTlc is in hexagonal platelet-like sheets and the particle size is about 1 μm. From the XRD patterns of Sr–Nd-HTlc calcination product, we only observe the phases of spinel and MgO and don't find the phases of SrO and Nd<sub>2</sub>O<sub>3</sub>, which show that Sr and Nd embedded into the crystal lattice of Sr–Nd-HTlc still occur in the structure of spinel.

**Keywords** Strontium · Neodymium · Separation · High level liquid waste · Hydrotalcite · In-situ synthesis

## Introduction

Nuclear energy plays an important role in energy generation of the modern society [1]. But the development of nuclear power industry is accompanied by increasing accumulation of high level liquid waste (HLLW), which contains long-lived minor actinides such as <sup>239</sup>Pu(III) and U(IV) as well as some specific fission product elements, such as <sup>90</sup>Sr(II), <sup>137</sup>Cs(I), <sup>99</sup>Tc(II), etc. [2, 3]. These radionuclides have persistent long radioactivity and biological toxicity, which makes a huge damage to humans, plants and animals [4, 5]. Thus, the safe disposal of HLLW has attracted numerous attentions [6].

The safe disposal of HLLW generally includes two steps, the first is to separate the long-lived actinides and specific fission product elements (<sup>90</sup>Sr, <sup>137</sup>Cs) from original HLLW, and the second is to immobilize these separated radionuclides to form a highly stable solid such as synroc, ceramic and glass [7, 8]. There are many separation methods of radionuclides, such as liquid–liquid solvent extraction, ion-exchange, adsorption, liquid membrane extraction and precipitation, etc [9–11]. The current attention has been focused on the liquid–liquid solvent extraction, which has shown high selectivity and extraction ability for radionuclides. However, this method usually generates a lot of secondary organic waste and probably increases the number of the instruments and equipments used in the process [12, 13].

Hydrotalcite-like compound (HTlc) has the general formula of  $[M_{1-x}^{II}M_x^{III}(OH)_2]^{x+} [A^{n-}]_{x/n} \cdot yH_2O$ , where M<sup>II</sup> and M<sup>III</sup> are divalent and trivalent cations respectively, with A<sup>n-</sup> being interlayer anions [14]. As the categories of cations or the chemical ratio of divalent cations to trivalent cations can be adjusted in wide ranges, a series of hydrotalcite-like compounds can be obtained with different compositions [15, 16]. These compounds, when calcined at

S. Yu (✉) · C. Zha · F. Lu · X. Wei · K. Wang  
School of Chemical Engineering, Hefei University  
of Technology and Anhui Key Laboratory of Controllable  
Chemical Reaction & Material Chemical Engineering,  
Hefei 230009, Anhui, People's Republic of China  
e-mail: shmyu@hfut.edu.cn

high temperature ( $\geq 600$  °C), produce stable  $M^{II}M^{III}O_4$  spinel which is one of the main synroc radices for the radionuclide immobilization [17, 18]. Thus, the radionuclides in HLLW could be separated by in situ hydrotalcite synthesis and immobilized by spinel synroc prepared from the calcination of hydrotalcite.

The separation of Sr from HLLW by in situ hydrotalcite synthesis has been studied in our previous work [19]. This study aims to investigate the feasibility of the simultaneous separation of  $^{90}\text{Sr}$  and trivalent actinides (using  $^{88}\text{Sr}$  and Nd as the surrogates, respectively) since the number of radionuclides in HLLW is more than one. The main work of this study is to: (1) study the effect of different parameters on the separation efficiency of Sr and Nd, such as pH value,  $(\text{Sr} + \text{Mg})/(\text{Nd} + \text{Al})$  molar ratio and initial concentrations of Sr ( $C_{\text{Sr(II)}}$ ) and Nd ( $C_{\text{Nd(III)}}$ ); (2) characterize the Sr–Nd-HTlc samples by XRD, FT-IR and SEM; (3) simply discuss the phase assemblages of Sr–Nd-HTlc calcination product.

## Experimental

### Synthesis of Sr–Nd-HTlc

All chemicals were purchased in analytical purity and used as received without further purification. Sr–Nd-doped hydrotalcite-like compounds (Sr–Nd-HTlc) were synthesized by hydrothermal treatment. A solution of  $0.8 \text{ mol L}^{-1}$  NaOH and  $0.05 \text{ mol L}^{-1}$   $\text{Na}_2\text{CO}_3$  was added dropwise with vigorous stirring to another solution containing  $\text{Mg}(\text{NO}_3)_2$ ,  $\text{Al}(\text{NO}_3)_3$ ,  $\text{Sr}(\text{NO}_3)_2$  and  $\text{Nd}(\text{NO}_3)_3$  with a molar ratio to precipitate and adjust the pH. Then the mixed solution was transferred into Teflon lined stainless steel bombs and hydrothermally treated at  $150$  °C for 12 h. Afterwards the precipitate was filtered, washed and finally dried for 10 h at  $80$  °C. The filter liquid solution was used to determine the residual Sr and Nd concentrations. The solid was used for X-ray powder diffraction (XRD), Fourier transform infrared (FT-IR) and scanning electron microscope (SEM) analysis.

### Characterization methods

XRD data were collected in the  $2\theta$  range of  $5$ – $70^\circ$  on a Rigaku D/MAX2500VL/PC diffractometer using  $\text{Cu K}\alpha$  radiation. FT-IR spectrum was recorded on a THERMO NICOLET67 spectrophotometer using KBr pellet technique. SEM was performed on a JEOL JSM-6700F instrument at an acceleration voltage of 20 kV and a working distance of 10 mm. The concentrations of Sr and Nd in solutions were measured by THERMO ICAP6300 inductively coupled plasma emission spectrometer.

## Results and discussion

### Acid–base titration

The variable pH values play a key role in the synthesis of Sr–Nd-HTlc, because it can directly affect the successful synthesis of HTlc with unique crystal form [20]. A mixed solution containing  $\text{Sr}^{2+}$ ,  $\text{Nd}^{3+}$ ,  $\text{Mg}^{2+}$  and  $\text{Al}^{3+}$  with a molar ratio was titrated by  $1.0 \text{ mol L}^{-1}$  NaOH solution at a constant rate under vigorous stirring. During the titration process, the pH value increased, and precipitation was formed in the system step by step. The variation plot of the pH value versus the added amount of NaOH is shown in Fig. 1.

According to Fig. 1, three different plateaus of pH values can be detected, i.e., 3.7–4.8, 8.5–11.0 and 13.3–14.0. At the first plateau, the hydrolyzation and polymerization of  $M^{III}$  mainly occurred. At the third plateau, the  $M^{II}$  precipitated in the form of  $M^{II}(\text{OH})_2$ . At the middle plateau, Sr–Nd-HTlc was obtained, indicating that the HTlc phase is more stable under this pH range than a mixture of  $M^{III}(\text{OH})_3$  and  $M^{II}(\text{OH})_2$  [21]. Thus, the synthesized pH range is chosen at 8.5–11.0 to obtain Sr–Nd-HTlc samples.

### Effect of pH value on the separation efficiency of Sr and Nd

The effect of pH value on the removal rates of Sr and Nd is shown in Fig. 2. As can be seen from Fig. 2, the higher pH value contributes to increasing removal rate of Sr. At pH 10.0–12.0, the removal rate of Sr approaches to an ultimate figure of 99 %. However, it is obviously that the pH value almost has no effects on the separation of Nd, and its removal rate maintains 99 % in the pH range of 6.0–12.0.

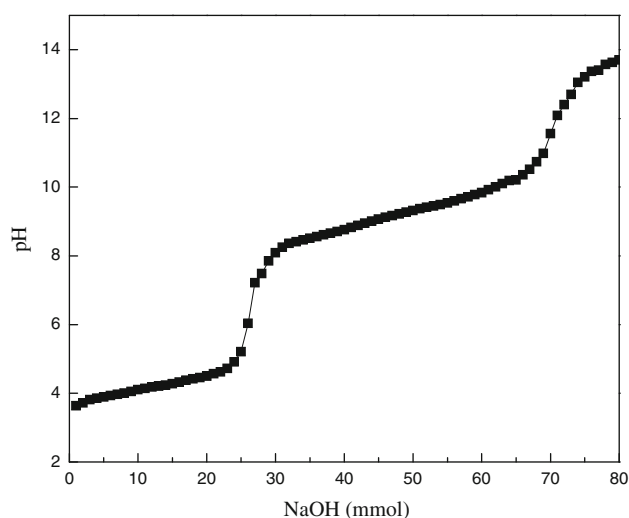


**Fig. 1** Evolution of pH versus NaOH (mmol) during the basic titration of solution,  $(\text{Sr} + \text{Mg})/(\text{Nd} + \text{Al})$  molar ratio = 3.0, initial  $C_{\text{Sr(II)}} = 70 \text{ mg L}^{-1}$ , initial  $C_{\text{Nd(III)}} = 50 \text{ mg L}^{-1}$

This trend maybe due to the fact that Nd can easily hydrolyze and polymerize at lower pH.

The XRD patterns of samples obtained at different pH are displayed in Fig. 3. All the samples present the main reflections of planes (003), (006), (012), (110) and (113) of hydroxalcite (JCPDS 70-2151) [22]. These sharp and symmetric peaks demonstrate the formation of a single well-crystallized Sr–Nd-HTlc at pH 9 and 11. Little impurities such as AlO(OH) (JCPDS 21-1307) and  $\text{Nd}_2(\text{CO}_3)_3 \cdot 8\text{H}_2\text{O}$  (JCPDS 53-0694) can be observed in the samples at pH 6, 7 and 12. The presence of  $\text{Nd}_2(\text{CO}_3)_3 \cdot 8\text{H}_2\text{O}$  indicates that the Nd separated from HLLW isn't all embedded into the structure of hydroxalcite. After calcination, the  $\text{Nd}_2(\text{CO}_3)_3 \cdot 8\text{H}_2\text{O}$  will transform into  $\text{Nd}_2\text{O}_3$ , which will markedly affect the immobilization efficiency of Nd. The main aim of our study is to obtain unique hydroxalcite phase and higher removal rates of simulated radionuclides, thus the optimal pH range is chosen to 10–11.

Effect of (Sr + Mg)/(Nd + Al) molar ratio on the separation efficiency of Sr and Nd

Figure 4 displays the effect of (Sr + Mg)/(Nd + Al) molar ratio on the removal rates of Sr and Nd. It is evident that the removal rates of Sr and Nd increase sharply when the (Sr + Mg)/(Nd + Al) molar ratio  $\leq 2.5$ , then they rise slowly and reach the ultimate point of 99 % when the (Sr + Mg)/(Nd + Al) molar ratio is 3.0. Change in removal rates of Sr and Nd might be attributed to the relative similar ionic radii of Sr and Nd to Mg ( $\text{Mg}^{2+}$  0.72 Å;  $\text{Al}^{3+}$  0.54 Å;  $\text{Sr}^{2+}$  1.18 Å; and  $\text{Nd}^{3+}$  0.98 Å) [23]. Thus with the increasing (Sr + Mg)/(Nd + Al) molar ratio,

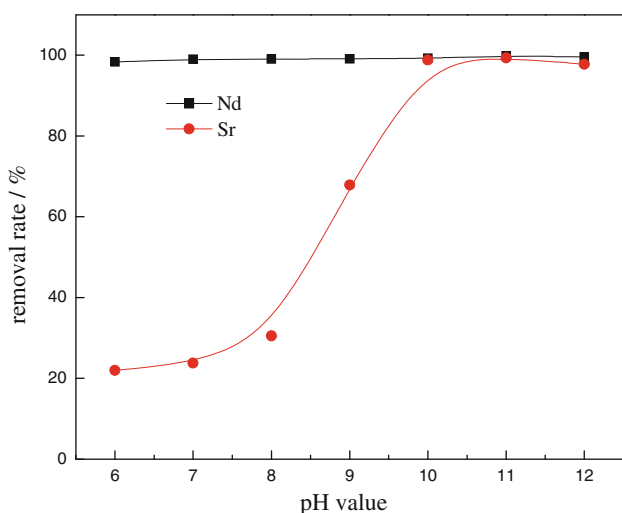


**Fig. 2** Effect of pH value on the removal rates of Sr and Nd, (Sr + Mg)/(Nd + Al) molar ratio = 3.0, initial  $C_{\text{Sr(II)}} = 70 \text{ mg L}^{-1}$ , initial  $C_{\text{Nd(III)}} = 50 \text{ mg L}^{-1}$

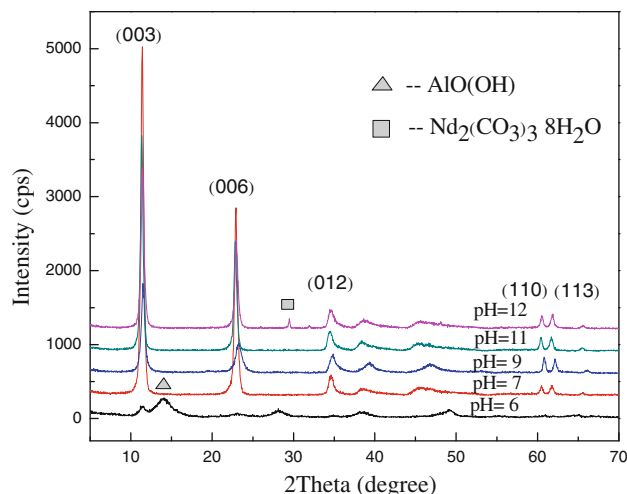


**Fig. 3** XRD patterns of synthetic samples in different pH values

which means the increase in molar quantity of Mg, the incorporation amounts of Sr and Nd increase based on the isomorphous replacement.

The XRD patterns of the samples under different (Sr + Mg)/(Nd + Al) molar ratios are shown in Fig. 5. As can be seen from Fig. 5, there is a single hydroxalcite phase existed in the synthetic sample when (Sr + Mg)/(Nd + Al) molar ratio is 3. However, the patterns obtained in other (Sr + Mg)/(Nd + Al) molar ratios exhibit the diffraction signals of AlO(OH),  $\text{Sr}(\text{OH})_2 \cdot \text{H}_2\text{O}$  (JCPDS 28-1222) and  $\text{Nd}_2(\text{CO}_3)_3 \cdot 8\text{H}_2\text{O}$ . Therefore, the (Sr + Mg)/(Nd + Al) molar ratio must be fixed to around three in order to assure the higher removal rates and unique hydroxalcite phase of Sr–Nd-HTlc.

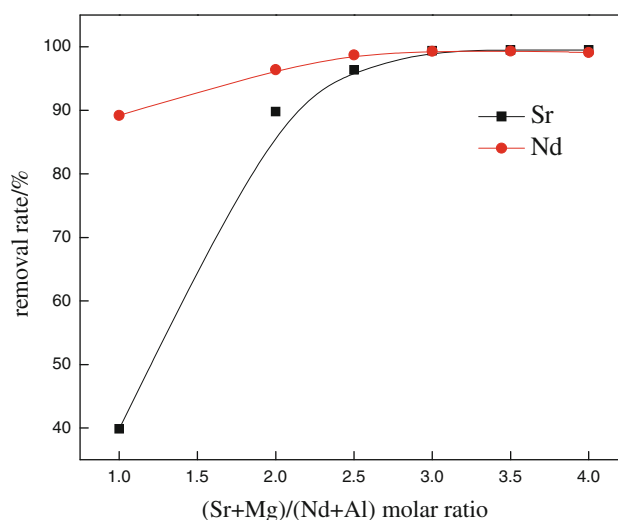


**Fig. 4** Effect of (Sr + Mg)/(Nd + Al) molar ratio on the removal rates of Sr and Nd, initial  $C_{\text{Sr(II)}} = 70 \text{ mg L}^{-1}$ , initial  $C_{\text{Nd(III)}} = 50 \text{ mg L}^{-1}$ , pH 11

Effect of initial  $C_{\text{Sr(II)}}$  and  $C_{\text{Nd(III)}}$  on the separation efficiency of Sr and Nd

The effect of initial  $C_{\text{Nd(III)}}$  on the removal rates of Sr and Nd is shown in Fig. 6. It can be clearly seen from the figure that with the increase in the initial  $C_{\text{Nd(III)}}$ , the removal rate of Sr does not appreciably decrease when the initial  $C_{\text{Sr(II)}}$  keeps an amount of  $70 \text{ mg L}^{-1}$ . It also can be observed that the removal rate of Nd decrease evidently with the increasing of the initial  $C_{\text{Nd(III)}}$ . These behaviors may be due to the limited substitution of Sr and Nd.

Figure 7 shows the effect of initial  $C_{\text{Sr(II)}}$  on the removal rates of Sr and Nd. It is clear that both the removal rates of Sr and Nd decrease slightly with increasing of the initial  $C_{\text{Sr(II)}}$  when the initial  $C_{\text{Sr(II)}} \leq 90 \text{ mg L}^{-1}$  and the initial  $C_{\text{Nd(III)}}$  keeps  $70 \text{ mg L}^{-1}$ . And when the initial  $C_{\text{Nd(III)}} \geq 90 \text{ mg L}^{-1}$ , they decrease rapidly. The result indicates that the effect of initial  $C_{\text{Sr(II)}}$  on Sr separation is similar to the influence of initial  $C_{\text{Nd(III)}}$  on Nd.

The XRD patterns of synthetic samples under different initial  $C_{\text{Sr(II)}}$  and  $C_{\text{Nd(III)}}$  are presented in Fig. 8. The samples have pure hydrotalcite crystal structure at initial  $C_{\text{Sr(II)}} = 70 \text{ mg L}^{-1}$ , initial  $C_{\text{Nd(III)}} = 60 \text{ mg L}^{-1}$  and initial  $C_{\text{Sr(II)}} = 90 \text{ mg L}^{-1}$ , initial  $C_{\text{Nd(III)}} = 70 \text{ mg L}^{-1}$ . No  $\text{AlO(OH)}$  or  $\text{Nd}_2(\text{CO}_3)_3 \cdot 8\text{H}_2\text{O}$  phase can be observed under these two conditions. Additionally, both the removal rates of Sr and Nd could reach more than 99 % at initial  $C_{\text{Sr(II)}} = 90 \text{ mg L}^{-1}$  and initial  $C_{\text{Nd(III)}} = 70 \text{ mg L}^{-1}$ . The above data suggest that the optimum initial  $C_{\text{Sr(II)}}$  and  $C_{\text{Nd(III)}}$  are 90 and  $70 \text{ mg L}^{-1}$  respectively.

The lattice parameters of hydrotalcites under different initial  $C_{\text{Sr(II)}}$  and  $C_{\text{Nd(III)}}$  are calculated and presented in Table 1. The lattice parameter  $a$ , which depends on the size

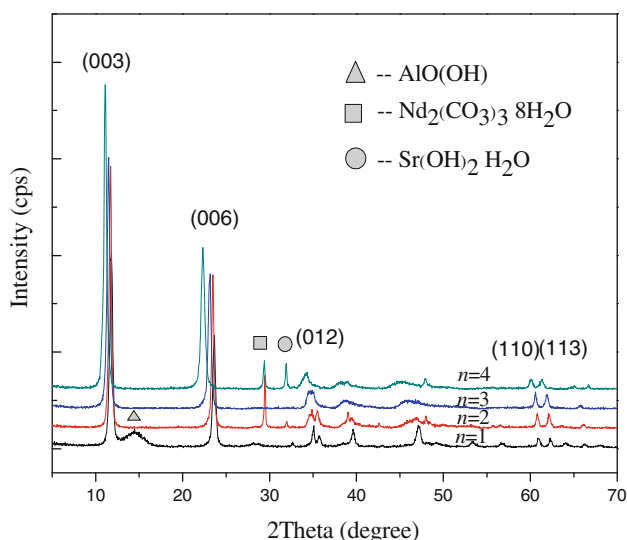


**Fig. 5** XRD patterns of synthetic samples under different  $(\text{Sr} + \text{Mg})/(\text{Nd} + \text{Al})$  molar ratios

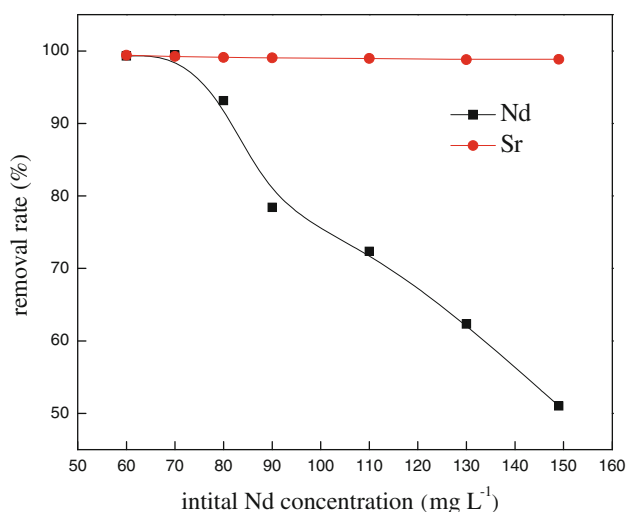


**Fig. 6** Effect of initial  $C_{\text{Nd(III)}}$  on the removal rates of Sr and Nd at initial  $C_{\text{Sr(II)}} = 70 \text{ mg L}^{-1}$ , pH 11,  $(\text{Sr} + \text{Mg})/(\text{Nd} + \text{Al})$  molar ratio = 3.0

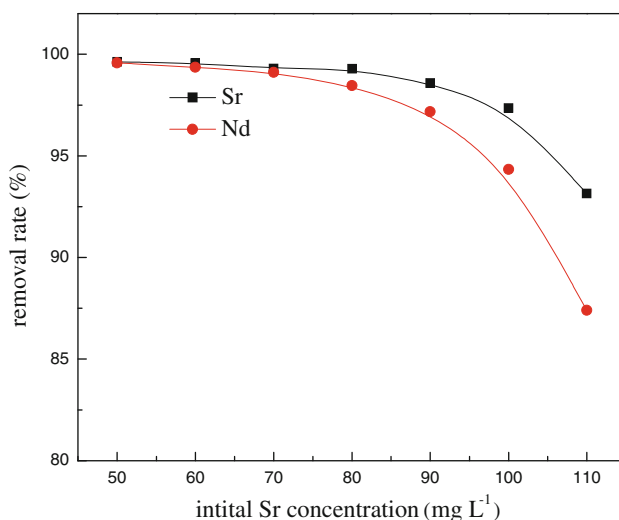


**Fig. 7** Effect of initial  $C_{\text{Sr(II)}}$  on the removal rates of Sr and Nd at initial  $C_{\text{Nd(III)}} = 70 \text{ mg L}^{-1}$ , pH 11,  $(\text{Sr} + \text{Mg})/(\text{Nd} + \text{Al})$  molar ratio = 3.0

of the cation in the brucite-like layers, is calculated by the expression  $a = 2d_{(110)}$ ; parameter  $c$  is related to the distance between brucite-like layers and can be obtained from the expression  $1/2\{d_{(003)} + [2d_{(006)}]\}$  [24]. As observed from Table 1, the lattice parameter  $a$  increases with the increase of initial  $C_{\text{Sr(II)}}$  and  $C_{\text{Nd(III)}}$ , which suggests that Sr and Nd incorporated into the lattice of HTlc.

#### FT-IR spectrum and SEM image

FT-IR spectrum of synthetic Sr–Nd-HTlc is shown in Fig. 9. A broad absorption band centered at  $3,573 \text{ cm}^{-1}$  can be attributed to O–H stretching vibration of

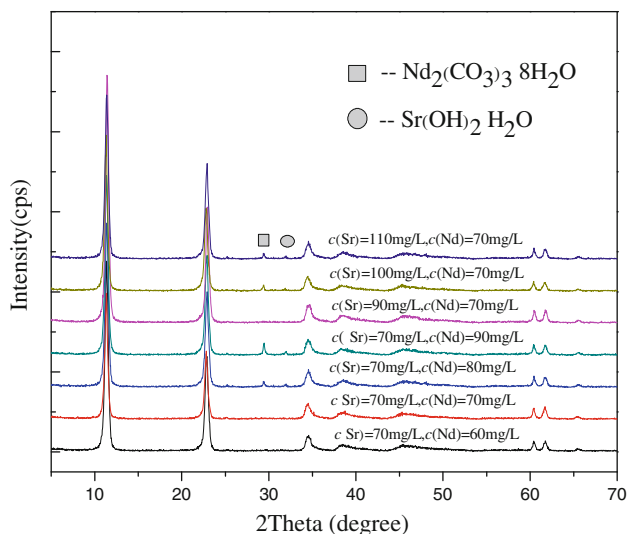


**Fig. 8** XRD patterns of synthetic samples under different initial  $C_{Sr(II)}$  and  $C_{Nd(III)}$

**Table 1** Crystallographic parameters of HTlc at different initial  $C_{Sr(II)}$  and  $C_{Nd(III)}$

Sample	Initial $C_{Sr(II)}$ (mg L <sup>-1</sup> )	Initial $C_{Nd(III)}$ (mg L <sup>-1</sup> )	<i>a</i> (Å)	<i>c</i> (Å)
HTlc-0	0	0	3.0576	23.1674
HTlc-1	110	70	3.0648	23.4539
HTlc-2	100	70	3.0622	23.4162
HTlc-3	90	70	3.0620	23.3319
HTlc-4	70	60	3.0587	23.1938
HTlc-5	70	70	3.0607	23.2934
HTlc-6	70	80	3.0608	23.3167
HTlc-7	70	90	3.0811	23.4413

hydrogen-bonded hydroxyl groups in the brucite-like sheets and of water in the interlayer space [25]. Another band at 1,623 cm<sup>-1</sup> is owing to the bending vibration of H–O–H and it should be assigned to the adsorbed water molecule in the interlayer. The peak observed at 1,367 cm<sup>-1</sup> can be indexed to CO<sub>3</sub><sup>2-</sup> ions [26]. The bands at 661 and 549 cm<sup>-1</sup> coincide by position and intensity ratio with the characteristic vibrations of hydrotalcite [27].

Figure 10 displays the SEM image of Sr–Nd-HTlc. It can be seen that the morphology of Sr–Nd-HTlc is in hexagonal platelet-like sheets [28] and its particle size is about 1 μm.

The characterization of calcined Sr–Nd-HTlc

Figure 11 shows the XRD pattern of the sample obtained from calcination of Sr–Nd-HTlc at 1,100 °C for 3 h. The peaks at 19.1, 31.3, 36.9, 44.8, 55.6, 59.4 and 65.3 could be assigned to the (110), (220), (311), (400), (422), (511) and (440) diffractions of spinel. Nevertheless, there is a small

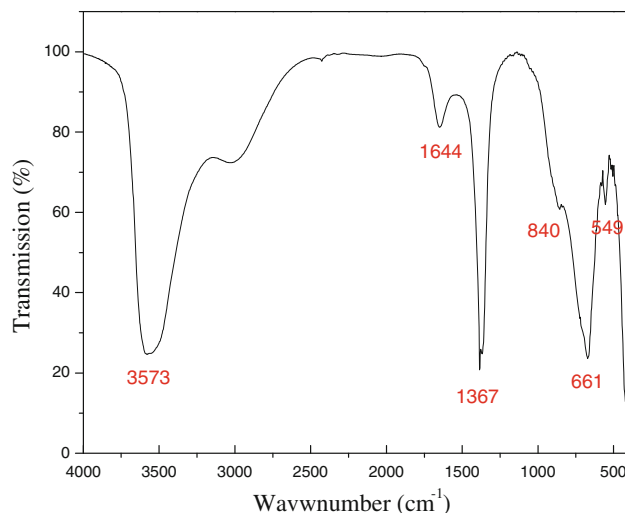


**Fig. 9** FT-IR spectra of Sr–Nd-HTlc

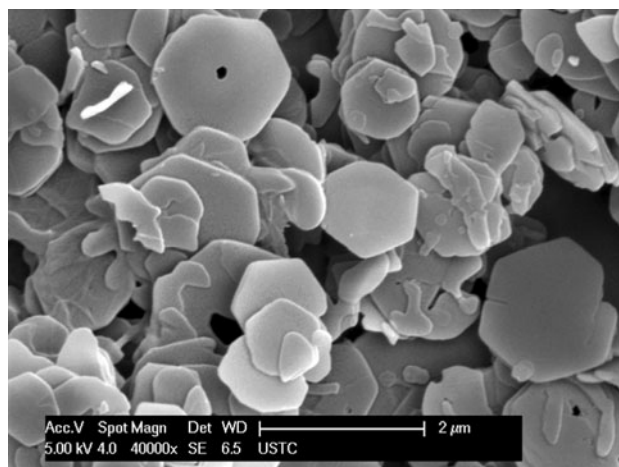


**Fig. 10** SEM image of Sr–Nd-HTlc

amount of MgO in the sample due to the excess of Mg in Sr–Nd-HTlc. The absence of SrO and Nd<sub>2</sub>O<sub>3</sub> in the product suggests that Sr and Nd embedded into the crystal lattice of Sr–Nd-HTlc still occurred in the structure of spinel.

**Conclusions**

In summary, Sr and Nd are successfully separated from the simulated liquid waste with a unique hydrotalcite phase and optimal removal rates of 99 % by in situ Sr–Nd-HTlc synthesis. The pH value, (Sr + Mg)/(Nd + Al) molar ratio and initial concentrations have great influences on the formation of Sr–Nd-HTlc and removal rates of Sr and Nd. The optimum conditions determined by acid–base titration, single factor tests and XRD analysis are that the initial  $C_{Sr(II)}$  and  $C_{Nd(III)}$  are 90 and 70 mg L<sup>-1</sup> respectively, pH range is 10–11 and (Sr + Mg)/(Nd + Al) molar ratio is around 3. Under these

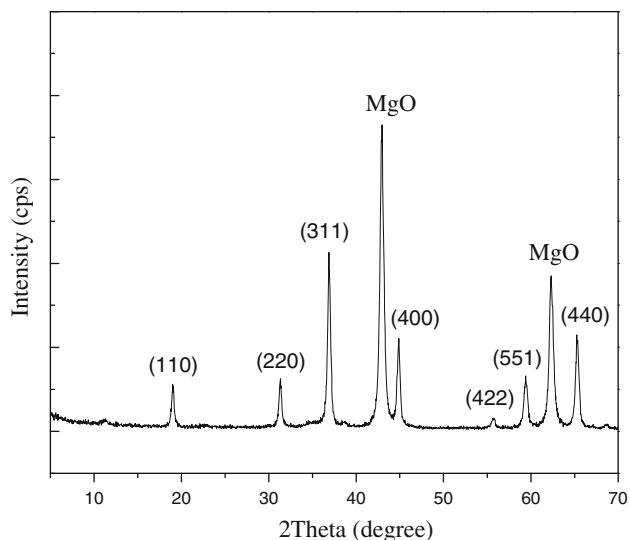


**Fig. 11** XRD patterns of calcined Sr-Nd-HTlc

conditions, Sr and Nd not only can be separated simultaneously from the simulated liquid waste, but also are all embedded into the crystal lattice of Sr-Nd-HTlcs. The morphology of Sr-Nd-HTlc is in hexagonal platelet-like sheets and the particle size is about 1  $\mu\text{m}$ . The calcination product of Sr-Nd-HTlc consists of spinel and MgO, and we can not observe the phases of SrO and Nd<sub>2</sub>O<sub>3</sub>, which indicates that Sr and Nd embedded into the crystal lattice of Sr-Nd-HTlc occurred in the structure of spinel.

**Acknowledgments** Financial support from National Natural Science Foundation of China (20971033) is acknowledged.

## References

- Frois B (2008) Nuclear energy in a global context. *Nucl Phys A* 805:320–327
- Xu D, Chen CL, Wang XK (2006) Sorption and diffusion of <sup>90</sup>Sr<sup>2+</sup> in compacted bentonite investigated by a capillary method. *J Radioanal Nucl Chem* 267(2):357–362
- Zhang AY, Kuraoka E, Kumagai M (2006) Removal of Pd(II), Zr(IV), Sr(II), Fe(III), and Mo(VI) from simulated high level liquid waste by extraction chromatography utilizing the macroporous silica-based polymeric materials. *Sep Purif Technol* 50:35–44
- Kikuchi T, Goto I, Suzuki K (2005) Separation of actinoids from HLW by the calix arene compound impregnated silica ion-exchanger. *Prog Nucl Energy* 47:397–405
- Mezaguer M, Kamel N, Lounici H, Kamel Z (2013) Characterization and properties of *Pleurotus mutilus* fungal biomass as adsorbent of the removal of uranium(VI) from uranium leachate. *J Radioanal Nucl Chem* 295:393–403
- Wang TH, Chen CJ, Ou LY, Wei YY, Chang FL, Teng SP (2011) Cs sorption to potential host rock of low-level radioactive waste repository in Taiwan: experiments and numerical fitting study. *J Hazard Mater* 192:1079–1087
- Wallace W, Schulz E, Horwitz P (1994) Chemical pretreatment of nuclear waste for disposal. Plenum press, New York
- Bao W, Xu S, Li LY, Song CL, Zhang JR, Zhu YJ (2002) Solidification of Sr-containing stripping solutions in titanate ceramics. *J Nucl Mater* 301:237–241
- Murali MS, Raut DR, Prabhu DR, Mohapatra PK, Tomar BS, Manchanda VK (2012) Removal of Cs from simulated high-level waste solutions by extraction using chlorinated cobalt dicarbollide in a mixture of nitrobenzene and xylene. *J Radioanal Nucl Chem* 291:611–616
- Chen CL, Hu J, Xu D, Tan XL, Meng YD, Wang XK (2008) Surface complexation modeling of Sr(II) and Eu(III) adsorption onto oxidized multiwall carbon nanotubes. *J Colloid Interface Sci* 323:33–41
- Chen CL, Hu J, Shao DD, Li JX, Wang XK (2009) Adsorption behavior of multiwall carbon nanotube/iron oxide magnetic composites for Ni(II) and Sr(II). *J Hazard Mater* 164:923–928
- Zhang AY, Hu QH (2010) Adsorption of cesium and some typical coexistent elements onto a modified macroporous silica-based supramolecular recognition material. *Chem Eng J* 159:58–66
- Tan SH, Chen XG, Ye Y, Sun J, Dai LQ, Ding Q (2010) Hydrothermal removal of Sr<sup>2+</sup> in aqueous solution via formation of Sr-substituted hydroxyapatite. *J Hazard Mater* 179:559–563
- Pavel OD, Voianu RZ, Rjega RB, Angelescu E (2010) Impact of the memory effect on the catalytic activity of Li–Al hydrotalcite-like compounds for the cyanoethylation reaction. *Mater Res Bull* 45:1106–1111
- Pérez-Ramírez J, Mul G, Moulijn JA (2001) In situ Fourier transform infrared and laser Raman spectroscopic study of the thermal decomposition of Co  $\pm$  Al and Ni  $\pm$  Al hydrotalcites. *Vib Spectrosc* 27:75–88
- Oliveira ELG, Grand CA, Rodrigues AE (2008) CO<sub>2</sub> sorption on hydrotalcite and alkali-modified (K and Cs) hydrotalcites at high temperatures. *Sep Purif Technol* 62:137–147
- Ma W, Zhao NN, Yang G, Tian LY, Wang R (2011) Removal of fluoride ions from aqueous solution by the calcination product of Mg–Al–Fe hydrotalcite-like compound. *Desalination* 268:20–26
- Ringwood AE, Kesson SE, Ware NG, Hibbertson W, Major A (1979) Immobilization of high-level nuclear reactor waste in synroc. *Nature* 278:219–223
- Lu FF, Yu SM, Qiu Y, Le JD, Wang HL, Wang XK (2012) Separation of simulated radionuclide Sr by in situ synthesis of hydrotalcite. *Acta Sci Circumst* 32(6):1388–1393 (in Chinese)
- Yan K, Xie XM, Li JP, Wang XL, Wang ZZ (2007) Preparation, characterization, and catalytic application of MgCoAl-hydrotalcite-like compounds. *J Nat Gas Chem* 16:371–376
- Boclair JW, Brateman PS (1999) Layered double hydroxide stability relative stabilities of layered double hydroxides and their simple counterparts. *Chem Mater* 11:298–302
- Vizca'no AJ, Lindo M, Carrero A, Calles JA (2011) Hydrogen production by steam reforming of ethanol using Ni catalysts based on ternary mixed oxides prepared by coprecipitation. *Int J Hydrogen Energy* 37(2):1985–1992
- Shannon RD (1976) Revised effective ionic radii and systematic studies of interatomic distances in halides and chalcogenides. *Acta Crystallogr A* 32:751–767
- Das J, Das D, Parida KM (2006) Preparation and characterization of Mg–Al hydrotalcite-like compounds containing cerium. *J Colloid Interface Sci* 301:569–574
- Wang J, You J, Li ZS, Yang PP, Jing XY, Zhang ML (2008) Preparation and characterization of new magnetic Co–Al HTLc/Fe<sub>3</sub>O<sub>4</sub> solid base. *Nanoscale Res Lett* 3:338–342
- Zhai RS, Das A, Hsu CK, Han CC, Canteenwala T, Chiang LY, Chuang TJ (2004) Polymeric fullerene oxide films produced by decomposition of hexanitro[60]fullerene. *Carbon* 42:395–403
- Islam M, Patel R (2011) Physicochemical characterization and adsorption behavior of Ca/Al chloride hydrotalcite-like compound towards removal of nitrate. *J Hazard Mater* 190:659–668
- Li ZS, You J, Wang J, Yang PP, Jing XY, Zhang ML (2009) Synthesis and characterization of tungstophosphoric acid intercalated Ni/Al HTLc with magnetite. *J Mater Process Technol* 209:2613–2619